Original research paper

Active omni wheel possessing seamless periphery and omnidirectional vehicle using it

Tatsuro Terakawa[a], Masaharu Komori[a,*], Yuuta Yamaguchi[a], and Yugo Nishida[a]

[a] Department of Mechanical Engineering and Science, Kyoto University, Kyoto daigaku-katsura, Nishikyo-ku, Kyoto 615-8540, Japan

* Corresponding author: komorim@me.kyoto-u.ac.jp (M. Komori).

Phone and fax: +81 75 383 3587

Abstract

Vehicles that are capable of achieving omnidirectional movement will work very efficiently in factories and warehouses. To meet this requirement, various omnidirectional vehicles have been proposed, but the wheel mechanism makes precise movement difficult. The active omni wheel (AOW), which can drive itself in an arbitrary direction at any time, can address this issue, but our previous design had mechanical vibration and acoustic noise due to gaps in the outer circumference of the wheel, and its complicated structure had a large number of parts. To solve these problems, this study developed a new AOW possessing a seamless periphery and simple structure. By using barrel-shaped friction-driven outer rollers arranged alternately on the left and right sides of the wheel, gaps between the outer rollers are eliminated and a smooth periphery is realized. Additionally, the power transmission paths were simplified to reduce the number

of parts. This paper explains the AOW structure and then presents analyses of structural conditions and kinematics of the AOW. A two-wheel-drive omnidirectional vehicle using the AOW was built and kinematically analyzed. Finally, experiments using the developed AOW and vehicle were conducted and their effectiveness was verified.

Keywords

omnidirectional movement, wheel, vehicle, kinematics, mechanism

1. Introduction

To increase efficiency for transporting products, vehicles, such as conveyance carriers and mobile robots, are used in factories and warehouses. The conventional vehicles combine going forward/backward and steering to realize various motions. However, the vehicles need switchbacks and turnabouts to move in different directions (right, left, or diagonally), which disrupts efficient motion in environments with narrow passages or many obstacles. Thus, omnidirectional vehicles that can move in the crosswise and diagonal directions directly, in addition to front-back direction and steering, are required.

To meet this requirement, various mechanisms for omnidirectional movement have been proposed and studied. One major example is the omni-wheeled vehicle [1]–[5]. An omni wheel has rollers embedded in its circumference. The axes of these rollers are lying on the wheel plane, and they rotate passively and freely. Thus, the

omni wheel can travel actively in one direction when a motor rotates the main body of the wheel and slide passively in a direction perpendicular to the wheel plane when the wheel receives a side force that rotates the rollers accordingly. By using three or more omni wheels, an omnidirectional vehicle can be constructed. The Mecanum wheel has a structure similar to that of the omni wheel, but the axes of the rollers are tilted away from the wheel plane [6]–[10]. This structure expands the flexibility for arranging the wheels in an omnidirectional vehicle. Orthogonal wheels utilize two parallel sphere-like-shaped rollers rotating actively in one direction and passively in a perpendicular direction [11]–[15]. Its movement principle is similar to those of the omni and Mecanum wheels. Another alternative for omnidirectional movement is the spherical wheel [16]–[20]. In a spherical wheel, the drive mechanism, usually using omni wheels, rotates a ball contacting the ground in a desired arbitrary direction. There is also the sphere-shaped wheel that can move actively in one direction and passively in another direction, just like the omni wheels [21]. These wheel mechanisms bring omnidirectional mobility to the vehicle, but it can be difficult for such vehicles to move precisely because resistance as a result of friction and viscosity that change depending on the conditions disturbs the passive rotation of the rollers in the wheels.

To address this issue, the locomotion mechanisms that can actively travel in an arbitrary direction have been proposed. For example, Omni-Crawler is a spherocylindrical crawler rotatable around the longitudinal axis [22]. The Omni-Crawler, as well as the spherical wheels, has an isotropic wheel radius in the longitudinal and lateral directions. It can provide an advantage in climbing steps crosswise but leads to a disadvantage in downsizing. Some of the authors

developed a disk-shaped wheel mechanism called an active omni wheel (AOW) [23]. The AOW utilizes a differential gear mechanism to rotate actively not only the main body of the wheel but also the outer rollers arranged around its circumference. A prototype AOW was built (Fig. 1), and experiments verified that it could accurately control its motion in an arbitrary direction. An omnidirectional driving wheel based on a screw-type differential rotating mechanism has also been proposed [24]. These wheel mechanisms have disk shapes like conventional wheels, which can be more suitable for arrangement in vehicles.

However, the previously developed AOW had vibration and noise problems because the outer roller arrangement and transmission system structure had gaps in between the outer rollers. Additionally, the large number of components was a problem. To solve these problems, this study developed a new AOW possessing a seamless periphery. By using barrel-shaped, friction-driven outer rollers arranged in a staggered double row, gaps between the outer rollers in the circumference of the wheel were completely eliminated. At the same time, the number of the parts constituting the new AOW was reduced with respect to that in the previous AOW. In this paper, we explain the structures of the previous and new AOWs first. We describe analyses carried out to derive the structural conditions and kinematics of the new AOW. Then, a two-wheel-drive omnidirectional vehicle using the proposed AOW was designed and kinematically analyzed. A prototype vehicle using the AOW was fabricated, and experiments were conducted to verify the effectiveness of the AOW.

2. New active omni wheel (AOW) with seamless periphery

2.1 Conventional AOW

First, we explain the structure and motion of the AOW previously developed. Its structure is shown schematically in Fig. 2, where Fig. 2(a) is a cross-section of the AOW through the rotation axis of the main body of the wheel and Fig. 2(b) is a cross-section parallel to the main body of the wheel. The outer circumference of the AOW consists mainly of outer rollers. Inside the AOW, a differential gear mechanism composed of input and output bevel gears is installed. Each input bevel gear is connected to a motor by an input shaft, and the output bevel gear is connected to the outer roller drive system by an output shaft. The outer roller drive system links the output shaft with the outer rollers to transmit the rotation. All of the outer rollers are joined by rotational couplings, and they rotate simultaneously. Bearings are placed between the main body of the wheel and the input and output shafts.

Next, we explain the motion of the AOW. When the two input shafts are rotated by the motors at the same speed in the same direction, as shown in Fig. 3(a), the output shaft revolves around the same rotation axis as the input shafts (axis A), and consequently, the main body of the wheel also rotates around axis A. Then, the AOW travels in a forward or backward direction. Oppositely, when the two input shafts are rotated at the same speed in opposite directions, as shown in Fig. 3(b), the output shaft rotates around the axis in a radial direction (axis B). It rotates the outer rollers around their axes via the outer roller drive system. Then, the AOW

travels in a right or left direction. Accordingly, when the two input shafts are rotated at different speeds, the output shaft rotates around both axes A and B, and both the main body of the wheel and the outer rollers rotate at the same time. Then, the AOW travels in a diagonal direction. Thus, the AOW can travel actively in an arbitrary direction by appropriate rotations of the input shafts.

However, the structure of the AOW creates some problems. The outer circumference of the AOW consists of outer rollers arranged annularly. To avoid interference between neighboring outer rollers, they are separated by spaces. These spaces are also necessary to provide structural supports and drive systems for the outer rollers, as shown in Fig. 2(b). For these reasons, the outer circumference of the AOW does not form a smooth circle. This means that the distance between the axle and the ground varies as the main body of the wheel rotates, which causes vibration and noise from this vertical motion as the AOW moves forward, backward, or diagonally. To address this issue, previous AOW designs incorporated as many outer rollers as possible to make the gaps smaller, but this led to an increased number of parts.

2.2 Structure and motion of new AOW

To solve the problems in the conventional AOW, we develop a new AOW design, whose structure is shown schematically in Fig. 4. The new AOW has barrel-shaped outer rollers on both sides of the wheel. The figure shows the design where six outer rollers are installed. All outer rollers have the same shape with constant

surface curvature. These outer rollers are arranged alternately on the left and right sides of the wheel at equal intervals so as to make the circumference of the AOW, as seen from the side, form a full smooth circle. We call this circle the main wheel. Each outer roller has structural supports at both ends to rotate freely and contact a transmission roller in the middle. The drive mechanism of this AOW is basically the same as that of the conventional AOW: Rotation of the two input shafts drives a differential gear mechanism inside the AOW, which rotates the main body of the wheel and the transmission rollers.

Next, we explain the motion of the new AOW. When the two input shafts are rotated at the same speed in the same direction, the main body of the wheel rotates as shown in Fig. 3(a), and the AOW travels in a forward or backward direction. When the two input shafts rotate at the same speed in opposite directions, the transmission rollers rotate as shown in Fig. 3(b). The rollers transmit their rotation to the outer rollers by friction force because they are in contact, as indicated in Fig. 4. Then, the outer rollers rotate and consequently, the AOW can move to the right or left. When the two input shafts rotate at different speeds, both the main body of the wheel and the outer rollers rotate, and the AOW can travel diagonally. Thus, the new AOW can actively travel in an arbitrary direction just as well as the previous AOW design.

Here, we discuss the design concept of the new AOW. The objectives are summarized into the following two points: to realize seamless periphery for vibration suppression and to reduce the number of parts. Regarding the seamless periphery, we adopt the barrel-shaped roller as mentioned above. By staggering the

outer rollers on the left and right sides, the rollers eliminate the gaps created by the structural supports at both ends of each roller. Also, using friction instead of gears to drive the rollers eliminates the gaps previously required for the outer roller drive systems. Thus, the periphery of the new AOW forms a seamless circle without gaps between rollers, and the AOW can travel smoothly without vibration or noise. With respect to reduction in the number of parts constituting the AOW, the barrel shape of the outer rollers makes it easier to reduce the number of outer rollers in the periphery; as few as four rollers can be employed. The friction drive with the transmission rollers makes the outer roller drive system simpler than the gear-driven system. Additionally, the drive mechanism is shared by the outer rollers on both sides.

The concrete design specifications are explained in Section 5.

3. Analysis of AOW structure and motion

In this section, analyses to clarify the structural conditions and kinematical characteristics of the new AOW are described.

3.1 Geometry of outer rollers

The barrel-shaped outer rollers of the AOW do not have a constant radius. Here, we describe how we addressed this variation in radius. First, the radius at an

arbitrary section of the outer roller is calculated. According to Fig. 5, the radius r of the section at central angle ϕ from the section with maximum radius is represented by

$$r = r_{\max} - R(1 - \cos\phi), \quad -\frac{\pi}{N} \le \phi \le \frac{\pi}{N} , \tag{1}$$

where $r_{\max}$ is the maximum radius of the outer roller, R is the radius of the main wheel, and N is the number of the outer rollers in the AOW.

To allow the AOW to travel in a right or left direction, no matter what point of the outer roller contacts the ground, the radius of the outer roller needs to be larger than zero at all sections. Considering that the minimum radius exists at the ends of the outer rollers, that is, $\phi = \pm\pi/N$, this condition is given by

$$r_{\max} - R\left(1 - \cos\frac{\pi}{N}\right) > 0 \Leftrightarrow r_{\max} > R\left(1 - \cos\frac{\pi}{N}\right) . \tag{2}$$

In contrast, if the radius is too large, the outer rollers on the same side of the AOW interfere with each other. Such interferences occur either when the ends of the outer rollers interfere as in Fig. 6(a) or when the sections with maximum radius interfere as in Fig. 6(b). The condition for avoiding these situations is expressed as follows:

$$r_{\max} - R\left(1 - \cos\frac{\pi}{N}\right) < \frac{R}{4\cos\frac{\pi}{N}} \wedge r_{\max} < \frac{R}{2}$$

$$\Leftrightarrow r_{\max} < \min\left\{R\left(1 - \cos\frac{\pi}{N} + \frac{1}{4\cos\frac{\pi}{N}}\right), \frac{R}{2}\right\} . \tag{3}$$

Eqs. (2) and (3) give the fundamental geometrical condition of the outer rollers.

Based on the conditions derived above, we evaluate the radius variations of the outer roller. In the AOW, the radius of the outer roller varies according to the ground contact point, which causes velocity variation in the right or left directions when the outer roller rotates at a constant speed. Therefore, to travel in the right or left direction at a constant speed, the rotational speed of the outer rollers needs to change according to the ground contact point. It is preferable to keep such variations small during operation of the AOW. Then, we define the minimum to maximum radius ratio of the outer roller as

$$\rho = \frac{r_{\max} - R\left(1-\cos\frac{\pi}{N}\right)}{r_{\max}}\ , \tag{4}$$

and evaluate the available range of ρ under the conditions of Eqs. (2) and (3). As ρ approaches 1, these variations become smaller.

The calculation result is shown in Fig. 7, where the vertical and horizontal axes represent ρ and N, respectively. The lower limit of ρ determined by Eq. (2) is $\rho = 0$ and the upper limit of ρ determined by Eq. (3) is indicated by the bold black solid line in the graph. The region exceeding this line is no longer a candidate for the AOW design because the outer roller interferences occur. At each N, ρ can assume a value between these limits depending on $r_{\max}/R$. In the graph, the contour lines describe $r_{\max}/R$ for each ρ and N. Note that N is restricted to even numbers, but the points are joined to describe contour lines in the graph for clarity. The graph shows that the upper limit of ρ becomes large, that is, the radius variations of the outer rollers becomes small, when N is large: In the region where N is small, the upper limit of ρ increases remarkably according to the increase of N, while in the region where N is large, the upper limit of ρ

gradually approaches 1. Under the same value of ρ, $r_{\max}/R$ becomes small as N becomes large. For example, the schematics on the right illustrate the geometrical relation of the main wheel and the outer rollers corresponding to points A and B in the graph, which suggests that the radius of the outer rollers becomes small relative to the radius of the main wheel R when N becomes large. This decreases the horizontal width of the AOW. In contrast, increasing N, i.e., increasing the number of the outer rollers causes increasing the number of the parts constituting the AOW. Therefore, the number and size of outer rollers in the new AOW should be designed with this tradeoff in mind.

3.2 Kinematics of AOW

This section explains the kinematics of the AOW. When we set the velocity of the AOW in the forward/backward and right/left directions as v_y and v_x, respectively, and the angular velocities input to the two input shafts are ω_1 and ω_2, respectively, the relation of these velocities is given by

$$\begin{bmatrix} v_x \\ v_y \end{bmatrix} = \begin{bmatrix} \frac{r}{2n} & -\frac{r}{2n} \\ \frac{R}{2} & \frac{R}{2} \end{bmatrix} \begin{bmatrix} \omega_1 \\ \omega_2 \end{bmatrix}, \tag{5}$$

where $n \in \mathbb{R}$ represents the reduction ratio between the differential gear mechanism and the outer rollers [23].

Eq. (5) shows that v_x is proportionate to r. As mentioned in Section 3.1, the value of r varies according to the ground contact point. Therefore, the movement

of the AOW is affected by the radius variation when it travels in the right, left, or diagonal direction. Then, we derive the inputs for the AOW to travel at a constant velocity by compensating the variation of r. From Eqs. (1) and (5), the input angular velocities ω_1 and ω_2 to realize certain velocities v_x and v_y are calculated as follows:

$$\begin{bmatrix}\omega_1\\ \omega_2\end{bmatrix} = \begin{bmatrix}\frac{n}{r} & \frac{1}{R}\\ -\frac{n}{r} & \frac{1}{R}\end{bmatrix}\begin{bmatrix}v_x\\ v_y\end{bmatrix} = \begin{bmatrix}\frac{v_y}{R} + \frac{nv_x}{r_{\max}-R(1-\cos\phi)}\\ \frac{v_y}{R} - \frac{nv_x}{r_{\max}-R(1-\cos\phi)}\end{bmatrix} . \tag{6}$$

Time differentiation of Eq. (6) gives the input angular accelerations $\dot{\omega}_1$ and $\dot{\omega}_2$ as

$$\begin{bmatrix}\dot{\omega}_1\\ \dot{\omega}_2\end{bmatrix} = \begin{bmatrix}\frac{\dot{v}_y}{R} + \frac{n\dot{v}_x}{r_{\max}-R(1-\cos\phi)} + \frac{nv_xv_y\sin\phi}{\{r_{\max}-R(1-\cos\phi)\}^2}\\ \frac{\dot{v}_y}{R} - \frac{n\dot{v}_x}{r_{\max}-R(1-\cos\phi)} - \frac{nv_xv_y\sin\phi}{\{r_{\max}-R(1-\cos\phi)\}^2}\end{bmatrix} , \tag{7}$$

where the relation $R\dot{\phi} = v_y$ is used. Considering that the outer roller contacting the ground changes as the main wheel rotates, ϕ needs to be replaced to meet $-\pi/N \le \phi \le \pi/N$ according to circumstances, namely,

$$\phi \to \phi - \frac{2i\pi}{N}, \quad i \in \mathbb{Z} .$$

By using Eqs. (6) and (7), the inputs needed to drive the AOW at a constant velocity are calculated, and the result is shown in Fig. 8. Here, we choose the situation where the AOW travels diagonally at a constant velocity with $R = 0.15$ m, $r_{\max} = 0.04$ m, $n = 2/3$, $N = 6$, $v_x = v_y = \sqrt{2}/4$ m/s, and $\dot{v}_x = \dot{v}_y = 0$ m/s^2. The graphs show that the input angular velocity and acceleration need to

be changed according to the rotational angle of the main wheel. During diagonal travel, especially, the rotational angle of the main wheel changes over time, and therefore the inputs also must change. The graphs indicate that the absolute values of the input angular velocity and acceleration take maximums at $\phi = \pm\pi/N$, when the end of an outer roller contacts the ground. Before and after $\phi = \pm\pi/N$, the angular acceleration input needs to change discontinuously because the outer roller contacting the ground changes.

When the AOW travels at a constant speed in a forward, backward, right, or left direction (but not diagonally), Eq. (7) gives $\dot{\omega}_1 = \dot{\omega}_2 = 0$, and then the input angular velocity becomes constant over time. During right or left travel, however, the input rotational velocity needs to be changed according to the rotational angle of the main wheel as well as in Fig. 8(a) because v_x is proportionate to r. In contrast, forward or backward travel is not affected by the ground contact, because v_y is independent of r.

3.3 Acceleration limit of the new AOW

In the new AOW, the input angular velocity needs to be temporally changed depending on the direction of travel, as discussed above. However, motors can generally accelerate their rotation only within certain limits, which imposes a restriction on the variation of angular velocity that the motors can impart to the input shafts of the AOW. Accordingly, we evaluate the effect of the input angular acceleration limit on the velocity and acceleration of the AOW.

Differentiating Eq. (5) by time yields

$$\begin{bmatrix} \dot{v}_x \\ \dot{v}_y \end{bmatrix} = \begin{bmatrix} \frac{r}{2n}(\dot{\omega}_1 - \dot{\omega}_2) - \frac{v_x v_y \sin\phi}{r} \\ \frac{R}{2}(\dot{\omega}_1 + \dot{\omega}_2) \end{bmatrix} . \tag{8}$$

Here, we consider the situation where the AOW travels at speed v in direction θ, which is defined as $v_x = v\cos\theta$ and $v_y = v\sin\theta$. When the AOW accelerates with acceleration a in the same direction as the traveling direction, that is, $\dot{v}_x = a\cos\theta$ and $\dot{v}_y = a\sin\theta$, the following relations are given:

$$\begin{cases} a = \dot{v}_x\cos\theta + \dot{v}_y\sin\theta \\ \quad = \left(\frac{R\sin\theta}{2} + \frac{r\cos\theta}{2n}\right)\dot{\omega}_1 + \left(\frac{R\sin\theta}{2} - \frac{r\cos\theta}{2n}\right)\dot{\omega}_2 - \frac{\sin\phi\cos^2\theta\sin\theta}{r}v^2 \\ 0 = \dot{v}_x\sin\theta - \dot{v}_y\cos\theta \\ \quad = -\left(\frac{R\cos\theta}{2} - \frac{r\sin\theta}{2n}\right)\dot{\omega}_1 - \left(\frac{R\cos\theta}{2} + \frac{r\sin\theta}{2n}\right)\dot{\omega}_2 - \frac{\sin\phi\cos\theta\sin^2\theta}{r}v^2 \end{cases} . \tag{9}$$

Eliminating $\dot{\omega}_2$ from these two equations results in

$$a = \frac{Rr}{nR\cos\theta + r\sin\theta}\dot{\omega}_1 - \frac{nR\sin\phi\cos\theta\sin\theta}{r(nR\cos\theta + r\sin\theta)}v^2 . \tag{10}$$

Considering the symmetry, we focus on the region of $0° \le \theta \le 90°$ and $v \ge 0$. At this time, a monotonically increases with respect to $\dot{\omega}_1$. When we set the upper limits of the input angular accelerations as $\dot{\omega}_{1\max}$ and $\dot{\omega}_{2\max}$, that is to say,

$$|\dot{\omega}_1| \le \dot{\omega}_{1\max}, |\dot{\omega}_2| = \left|-\frac{nR\cos\theta - r\sin\theta}{nR\cos\theta + r\sin\theta}\dot{\omega}_1 - \frac{2n\sin\phi\cos\theta\sin^2\theta}{r(nR\cos\theta + r\sin\theta)}v^2\right| \le \dot{\omega}_{2\max} , \tag{11}$$

the maximum value of $\dot{\omega}_1$ is calculated as

$$\begin{cases} \min\left(\dot{\omega}_{1\max}, \frac{nR\cos\theta + r\sin\theta}{nR\cos\theta - r\sin\theta}\dot{\omega}_{2\max} - \frac{2n\sin\phi\cos\theta\sin^2\theta}{r(nR\cos\theta - r\sin\theta)}v^2\right) & \text{if} \quad \frac{nR}{r} > \tan\theta \\ \dot{\omega}_{1\max} & \text{if} \quad \frac{nR}{r} = \tan\theta \\ \min\left(\dot{\omega}_{1\max}, -\frac{nR\cos\theta + r\sin\theta}{nR\cos\theta - r\sin\theta}\dot{\omega}_{2\max} - \frac{2n\sin\phi\cos\theta\sin^2\theta}{r(nR\cos\theta - r\sin\theta)}v^2\right) & \text{if} \quad \frac{nR}{r} < \tan\theta \end{cases} . \quad (12)$$

By substituting Eq. (12) into Eq. (10), we obtain the maximum value of acceleration a.

The calculation results of the maximum acceleration at each pair of values for v and θ are shown in Fig. 9. The parameters used were $R = 0.15$ m, $r_{\max} = 0.04$ m, $n = 2/3$, and $N = 6$. The maximum input angular velocities were set as $\dot{\omega}_{1\max} = \dot{\omega}_{2\max} = 50\pi$ rad/s^2. Note that the maximum acceleration in the graph is normalized by using the ratio to the value at $v = 0$ m/s for each θ to compare the effect of the radius variation of the outer rollers on the traveling acceleration. The graph shows that the maximum acceleration monotonically decreases as v increases, except when $\theta = 0°$ and $90°$. This is because the input angular velocity needs to be changed periodically during diagonal travel, as shown in Fig. 8, and the required angular velocity becomes larger as v becomes larger. The value of v when the maximum acceleration is zero represents the maximum velocity of the AOW in each direction. The decrease of the maximum acceleration increases as θ approaches $45°$. Meanwhile, the maximum acceleration is constant independent of v at $\theta = 0°$ and $90°$ because the input angular velocity does not need to change temporally for non-diagonal travel (forward/backward and right/left). Thus, the maximum velocity and acceleration of the AOW are different depending on the direction of travel. Therefore, we need to design the AOW so that it can travel at the required speed in each direction. Furthermore, we need to select motors and generate commands that allow the maximum rotational acceleration to vary

depending on the rotational speed especially under high-speed and high-acceleration conditions.

4. Structure and kinematics of two-wheel-drive omnidirectional vehicle using AOW

The new AOW can be used to realize an omnidirectional vehicle that achieves planar motion with three degrees of freedom (DOF), including arbitrary-directional translation and turns. In this section, we discuss the structure and motion of the omnidirectional vehicle.

The AOW itself can move with two DOF actively. Therefore, to make a vehicle that moves with three DOF, a driving wheel with one active DOF is necessary in addition to the AOW. Moreover, for omnidirectional movement, the driving wheel must not impose nonholonomic constraints on the vehicle motion. For example, conventional wheels that can move in only one direction are unsuitable. By considering these conditions, we propose a two-wheel-drive vehicle with one AOW and one passive omni wheel (conventional omni wheel).

The vehicle's omnidirectional mobility is shown in Fig. 10, where the AOW and the omni wheel are arranged coaxially in parallel, as one example of possible wheel arrangement. The two input shafts of the AOW and one input shaft of the omni wheel are driven independently from each other, and each wheel can travel at an arbitrary velocity. When both wheels travel forward at the same speed, as

shown in Fig. 10(a), the vehicle moves forward. When the AOW travels to the right, as in Fig. 10(b), the omni wheel also travels to the right at the same speed because it travels on the passively rotating rollers. As a result, the vehicle moves to the right at a speed determined by the AOW. As shown in Fig. 10(c), when the AOW travels diagonally and the omni wheel travels forward in the forward direction component velocity of the AOW, the vehicle performs the diagonal translation. Fig. 10(d) shows that rotating the AOW and the omni wheel in opposite directions makes the vehicle turn. Thus, the vehicle can realize planar motion in three DOF, omnidirectional movement, by combining these movements.

Next, we discuss the motion of the proposed omnidirectional vehicle theoretically based on kinematics. Here, not only the wheel arrangement in Fig. 10 but also other configurations become the object of analysis. As shown in Fig. 11, each wheel is located at an angle α_j and distance d_j from the center of the vehicle directed at β_j, where $\alpha_j = 0$ corresponds to the right direction of the vehicle and $\beta_j = 0$ corresponds to the situation when the line passing through the centers of the vehicle and the wheel cross the wheel plane at right angles. The index $j = 1$ represents the parameters belonging to the AOW, and $j = 2$ represents the parameters belonging to the passive omni wheel. When we set the forward or backward velocity of the vehicle as V_Y, the right or left velocity as V_X, the angular velocity as Ω, and the forward or backward velocity of the omni wheel as v_w, the relation between the velocities of the wheels and the vehicle is given as follows:

$$A\begin{bmatrix} V_X \\ V_Y \\ \Omega \end{bmatrix} = \begin{bmatrix} v_y \\ v_x \\ v_w \end{bmatrix} \tag{13}$$

$$A = \begin{bmatrix} -\sin(\alpha_1 + \beta_1) & \cos(\alpha_1 + \beta_1) & d_1 \cos\beta_1 \\ \cos(\alpha_1 + \beta_1) & \sin(\alpha_1 + \beta_1) & d_1 \sin\beta_1 \\ -\sin(\alpha_2 + \beta_2) & \cos(\alpha_2 + \beta_2) & d_2 \cos\beta_2 \end{bmatrix} .$$

Eq. (13) expresses the kinematics of the proposed omnidirectional vehicle.

Based on the derived kinematics, we evaluate the wheel arrangement in the proposed omnidirectional vehicle. The determinant of the matrix A in Eq. (13) is calculated as

$$\begin{aligned} \det A &= d_1 \cos(\alpha_1 - \alpha_2 - \beta_2) - d_2 \cos\beta_2 \\ &= \{d_1 \cos(\alpha_2 - \alpha_1) - d_2\} \cos\beta_2 - d_1 \sin(\alpha_2 - \alpha_1) \sin\beta_2 \quad . \end{aligned} \tag{14}$$

When the determinant is zero, namely,

$$\det A = 0 \Leftrightarrow \tan\beta_2 = \frac{d_1 \cos(\alpha_2 - \alpha_1) - d_2}{d_1 \sin(\alpha_2 - \alpha_1)} \tag{15}$$

is given, Eq. (13) assumes a singular configuration where the forward kinematics is not established. At this time, the motion of the vehicle is not determined by any wheel velocity. The condition for Eq. (15) indicates the situation when the AOW is located in the wheel plane of the omni wheel, as shown in Fig. 12. In this case, the vehicle cannot control the rotation around the AOW at all. Therefore, in the design of the vehicle, the states of or near those shown in Fig. 12 must be avoided because the motion becomes unstable. In contrast, arranging the AOW and omni wheel in parallel achieves the state farthest from the singular configuration under the designated α_1, α_2, d_1, and d_2, and the vehicle is more likely to perform well. The wheel arrangement of the vehicle in Fig. 10 is one example. Additionally, $\det A$ expressed by Eq. (14) is equivalent to the distance between the wheel plane

of the passive omni wheel and the center point of the AOW. Then, the parameters α_1, α_2, d_1, and d_2 should be designed to make the distance as long as possible.

5. Development and testing of two-wheel-drive omnidirectional vehicle with new AOW

To verify that the new AOW installed in an omnidirectional vehicle performs as expected, a prototype was developed and tested.

5.1 Design and development of prototype

First, we explain the design specifications of the AOW prototype. Concerning the design objectives of the new AOW described in Section 2.2, we aim to reduce the magnitude of vibration caused by the gaps between the outer rollers to smaller than a tenth of that in the conventional AOW (Fig. 1), and to decrease the number of main parts necessary for the fundamental structure and function to the half or less. Besides them, we intend that the load capacity is greater than 900 N, the diameter of the AOW is smaller than 0.35 m (approximately 75% of the conventional AOW diameter), and the driving force capacity is larger than 200 N. The prototype is assumed to be used on flat ground. Based on these specifications, we designed the AOW prototype.

Fig. 13 shows the developed AOW. As shown in Fig. 13(a), its structure is

basically the same as the structure shown in Fig. 4. Six outer rollers are arranged alternately on the left and right sides at 60° intervals. Seen from the side, the arcs of the outer rollers are connected smoothly, which creates a circular wheel circumference. The transmission system shown in Fig. 13(b) is divided into three paths after the differential gear mechanism, each of which rotates the adjacent two transmission rollers. This means that the outer rollers on both sides share the same power transmission path because the transmission rollers are located on the same plane. Thus, the new AOW has fewer outer rollers, a simpler transmission system, and fewer parts than the conventional AOW shown in Fig. 1. With respect to the vibration and the number of the parts in the AOW, we make a quantitative evaluation in Section 5.3. The diameter of the developed AOW is 0.3 m, which meets the design specification. The material, size, and shape of each part are designed to satisfy the specifications of the load capacity and the driving force capacity. The parameters of the developed AOW are $R = 0.15$ m, $r_{\max} = 0.04$ m, and $n = 2/3$.

Fig. 14 shows the two-wheel-drive omnidirectional vehicle developed using the new AOW. The right driving wheel is the AOW and the left driving wheel is the passive omni wheel. These wheels are arranged in parallel and their axles are in the same vertical plane. The two input shafts of the AOW and the one input shaft of the omni wheel are driven independently by three motors. In addition to the driving wheels, supporting wheels are attached at the four corners of the vehicle to stabilize it horizontally. The supporting wheels are omni wheels whose main body of the wheel and rollers all rotate passively. The parameters of the developed vehicle are $\alpha_1 = 0°$, $d_1 = 0.275$ m, $\beta_1 = 0°$, $\alpha_2 = 180°$, $d_2 = 0.330$ m, and $\beta_2 =$

$-180°$. The sizes of other parts are as follows: The height from the ground to the seat is 0.55 m, the total width of the vehicle is 0.80 m, the radius of the driving omni wheel is 0.10 m, and the radii of the supporting omni wheels are 0.05 m.

Fig. 15 shows the structure of the control system hardware of the developed omnidirectional vehicle. The vehicle is operated using a three-axis joystick. The tilt and twist angles input with the joystick are sent to the controller and converted into the target velocity of the vehicle. The input angular velocity for each motor is generated from the target velocity using the inverse kinematics, such as Eqs. (6) and (13). The angular velocity commands are sent to each motor driver. The angular velocity commands are restricted not to exceed the limits of the rotational acceleration, as discussed in Section 3.3. The rotational angle of the main wheel of the AOW is measured by a rotary encoder and used in the calculation of the inverse kinematics.

5.2 Vehicle testing

Mobility testing of the developed vehicle is pictured in Fig. 16. In this experiment, a person rode on and operated the vehicle. The figure shows (a) forward translation, (b) right translation, (c) diagonal translation, and (d) turning. All of these movements were achieved as expected.

The input angular velocities of the AOW ω_1 and ω_2 need to be changed according to the changing ground contact point of the outer rollers during diagonal

translation, as discussed in Section 3. To demonstrate that this behavior was actually realized in the developed vehicle, we measured the rotational speeds of the motors with the rotary encoder attached to each motor, and compared them with the commanded values. Fig. 17 shows the measurement result when the target velocity was $V_X = V_Y = 0.28$ m/s, which is the same movement as in Fig. 16(c). The graph extracts the region where the velocity became almost constant after a certain period of time from the start at 0 s. It shows that the measured and commanded values of ω_1 and ω_2 agreed with each other and verifies that the developed mechanisms work according to the theory.

When we evaluate the result of Fig. 17 in detail by focusing on the peaks of ω_1 and ω_2, the measured values seem delayed compared to the commanded values by about 50 ms. Such delays cause a difference between the ground contact points of the outer rollers in the calculation and the actual state, which leads to errors in the right/left velocity of the vehicle V_X. Fig. 18 shows the simulation result of V_X when ω_1 and ω_2 are input with a 50-ms delay. The graph clarifies that V_X varies around the target value $V_X = 0.28$ m/s. In fact, the vehicle operator in the experiment perceived lateral vibration when moving diagonally. Regarding this issue, dynamics-based feedforward control is thought to be useful for solving the delay problem.

5.3 Comparison of conventional and new AOWs

To show the effectiveness of the developed new AOW, we compare it with the

conventional AOW shown in Fig. 1. The problem in the conventional AOW is that it has gaps between the outer rollers, which cause vibration during traveling, and it requires a large number of parts to make the gaps smaller. The new AOW is designed to solve these problems.

First, in order to evaluate the traveling vibration, we measured the vertical vibration of the vehicles equipped with the conventional and new AOWs (Figs. 1 and 14, respectively). An acceleration meter (Cosmic ME Co., Inc., Sorocaba-1) was fixed on the center of the upper plane of the vehicles after removing the seats. Sampling range was 20 m/s^2, the sampling rate was 1 ms, and the sampling number was $2^{14} = 16384$. The vehicles traveled forward at $V_Y = 0.3$ m/s. Fig. 19 shows the measurement result of the vibration spectra. In the figure, the dotted lines indicate the multiples of the specific frequency f of the vibration resulting from the gaps between the outer rollers. Namely, f is given by the following equation.

$$f = \frac{V_Y}{2\pi R} N \tag{16}$$

In the conventional AOW, $R = 0.23$ m and $N = 32$ is applied, and then $f = 6.57$ Hz is supposed. In the new AOW, $R = 0.15$ m and $N = 6$ result in $f = 1.91$ Hz.

Focusing on the vibration at the frequency of f, the conventional AOW caused a relatively large peak around 0.40 m/s^2, while the amplitude of the new AOW is even smaller than 0.01 m/s^2. This result suggests that the new AOW can suppress the vibration caused by the gaps between outer rollers as expected, and the design specification is satisfied. In the figure, the recommended amplitude limit proposed

by Janeway [25] is drawn by a black line as an example of an evaluation index. This limit represents the threshold between comfort and discomfort in human reactions to vibration. Here, the vibration of the conventional AOW is beyond the limit, which means that the vibration may make sensitive persons feel discomfort. The conventional AOW also assumes a peak close to the limit at the frequency of $2f$. On the other hand, though the vibration of the new AOW has a peak at the frequency of $3f$, its amplitude reaches no more than 11% of the limit. We must consider that the fair comparison of these results is difficult because the structures of the two vehicles are different and the factors other than the AOWs may affect the vibrations. Nevertheless, the fact that the vehicle with the new AOW can travel with small vibration verifies that the new AOW design can avoid the vibration problem of the conventional AOW as expected, and that it can be successfully incorporated into an omnidirectional vehicle.

Next, we compare the number of parts constituting the AOWs. Table 1 shows the number of main parts, i.e., the rollers, gears, couplings, shafts, outer roller's supports, and main body in each AOW. As the table shows, the number of each part in the new AOW is equal to or less than that of the conventional AOW. In total, the new AOW has less than a half of the parts the conventional AOW has. Thus, the design specification on the number of parts is satisfied. This is mainly because the new AOW does not need so many outer rollers to compensate the gaps as the conventional AOW does. When the number of the outer rollers is small, the number of the transmission paths in the AOW becomes small, and accordingly, the number of the parts such as the gears, shafts, and supports is kept small.

From the above results, we conclude that the new AOW design proposed in the present research achieves the objectives, that is, to realize seamless periphery for vibration suppression and to reduce the number of parts and that the design is effective to solve the problems of the conventional AOW.

6. Conclusion

If vehicles used in factories and warehouses achieve omnidirectional movement, they can move more smoothly and efficiently, even in limited space. To meet this requirement, some of the authors proposed the AOW, which can accurately travel in any direction. However, the conventional AOW has gaps between the outer rollers constituting the outer circumference of the wheel, and therefore vibration and noise occur while the AOW travels. At the same time, it needs a large number of parts. To solve these problems, this study developed a new AOW design possessing a seamless periphery and simpler structure. Through analyses of and experiments with the new AOW and an omnidirectional vehicle using it, we obtained the following results:

(1) We developed a new AOW without gaps between the outer rollers, which are barrel-shaped, friction-driven, and arranged alternately on the left and right sides of the wheel. This structure contributes to a simplified power transmission system and a reduction in the number of parts.

(2) Through analysis of the new AOW, the following aspects were clarified: the number and size of the outer rollers affect the velocity characteristics of the AOW, the input angular velocity and acceleration need to be temporally changed to travel

at a constant velocity, and the maximum acceleration of the AOW is restricted depending on the travel velocity and direction.
(3) A two-wheel-drive omnidirectional vehicle was developed using the new AOW and a passive omni wheel. Through kinematic analysis of the omnidirectional vehicle, it was clarified that its motion became stable when the wheels were arranged in parallel.
(4) The new AOW and omnidirectional vehicle were constructed and tested. Mobility testing verified that the developed vehicle could perform omnidirectional movement as expected. The measurement of the input angular velocity verified that its behavior in the diagonal travel was according to the theory unique to the new AOW. The comparison with the conventional AOW proved the effectiveness of the new AOW in reducing the vertical vibration and in decreasing the number of parts.

In future work, we plan to analyze and evaluate slippage between the transmission roller and outer roller in the proposed AOW for the sake of practicality.
Step-climbing should also be discussed considering the characteristics of the proposed mechanism.

Acknowledgments

This work was supported by the Japan Society for the Promotion of Science, JSPS Kakenhi Grant Number JP25289023.

References

[1] Fisette P, Ferriere L, Raucent B, Vaneghem B. A multibody approach for modelling universal wheels of mobile robots. Mechanism and Machine Theory 2000;35(3):329–51.

[2] de Best J, van de Molengraft R, Steinbuch M. A novel ball handling mechanism for the RoboCup middle size league. Mechatronics 2011;21(2):469–78.

[3] Tavakoli M, Viegas C. Analysis and application of dual-row omnidirectional wheels for climbing robots. Mechatronics 2014;24(5):436–48.

[4] Tavakoli M, Lourenço J, Viegas C, Neto P, de Almeida AT. The hybrid OmniClimber robot: Wheel based climbing, arm based plane transition, and switchable magnet adhesion. Mechatronics 2016;36:136–46.

[5] Santos J, Conceição A, Santos T, Araújo H. Remote control of an omnidirectional mobile robot with time-varying delay and noise attenuation. Mechatronics 2018;52:7–21.

[6] Saha SK, Angeles J, Darcovich J. The design of kinematically isotropic rolling robots with omnidirectional wheels. Mechanism and Machine Theory 1995;30(8):1127–37.

[7] Cooney JA, Xu WL, Bright G. Visual dead-reckoning for motion control of a Mecanum-wheeled mobile robot. Mechatronics 2004;14(6):623–37.

[8] Indiveri G. Swedish wheeled omnidirectional mobile robots: kinematics analysis and control. IEEE Transactions on Robotics 2009;25(1):164–71.

[9] Guo S, Jin Y, Bao S, Xi FF. Accuracy analysis of omnidirectional mobile manipulator with mecanum wheels. Advances in Manufacturing

2016;4(4):363−70.
[10] Yamada N, Komura H, Endo G, Nabae H, Suzumori K. Spiral mecanum wheel achieving omnidirectional locomotion in step-climbing. Proceedings of the IEEE international conference on advanced intelligent mechatronics 2017:1285–90.
[11] Kalmár-Nagy T, Ganguly P, D'Andrea R. Real-time trajectory generation for omnidirectional vehicles. Proceedings of the American control conference 2002:286−91.
[12] Mourioux G, Novales C, Poisson G, Vieyres P. Omni-directional robot with spherical orthogonal wheels: concepts and analyses. Proceedings of the IEEE international conference on robotics and automation 2006:3374–9.
[13] Ren C, Ma S. Generalized proportional integral observer based control of an omnidirectional mobile robot. Mechatronics 2015;26:36–44.
[14] Wang X, Cui W, Xu X, Ye C. Research on an omni-directional AGV with differential wheels. Proceedings of the IEEE international conference on mechatronics and automation 2016:1566−71.
[15] Yu S, Ye C, Liu H, Chen J. Development of an omnidirectional automated guided vehicle with MY3 wheels. Perspectives in science 2016;7:364–8.
[16] Kumagai M, Ochiai T. Development of a robot balanced on a ball —first report, implementation of the robot and basic control—. Journal of robotics and mechatronics 2010;22(3):348–55.
[17] Ishida S, Miyamoto H. Collision-detecting device for omnidirectional electric wheelchair. ISRN Robotics 2013:672826.
[18] Nagarajan U, Kantor G, Hollis R. The ballbot: An omnidirectional balancing mobile robot. The international journal of robotics research 2014;33(6):917–30.
[19] Hoshino T, Yazawa M, Naganuma R, Takada K. Design and implementation

of a personal mobility of single spherical drive. Journal of physics: conference series 2016;744:012211.
[20] Navabi H, Sadeghnejad S, Ramezani S, Baltes J. Position control of the single spherical wheel mobile robot by using the fuzzy sliding mode controller. Advances in fuzzy systems 2017:2651976.
[21] Tadakuma K, Tadakuma R, Berengueres J. Tetrahedral mobile robot with spherical omnidirectional wheel. Journal of Robotics and Mechatronics 2008;20(1);125-34.
[22] Tadakuma K, Tadakuma R, Nagatani K, Yoshida K, Peters S, Udengaard M, Iagnemma K. Crawler vehicle with circular cross-section unit to realize sideways motion. Proceedings of IEEE/RSJ International Conference on Intelligent Robots and Systems 2008:2422-8.
[23] Komori M, Matsuda K, Terakawa T, Takeoka F, Nishihara H, Ohashi H. Active omni wheel capable of active motion in arbitrary direction and omnidirectional vehicle. Journal of Advanced Mechanical Design, Systems, and Manufacturing 2016;10(6);JAMDSM0086.
[24] Nomura A, Fujita M, Fujimoto T, Nishimura A, Tetsui H, Takane E, Komatsu H, Tadakuma K, Tadakuma R, Konyo M, Tadokoro S. Screw-type differential rotating mechanism—realization of driving force transmitting mechanism in structuring the vehicle with 4 omnidirectional driving wheels—. Proceedings of the 18th SICE System Integration Division Annual Conference 2017:980-983.
[25] Society of Automotive Engineers. Vehicle Dynamics Committee. Ride and Vibration Data Manual. New York: SAE; 1965.

Fig. 1 Active omni wheel and omnidirectional vehicle developed in [23].

Fig. 2 Structure of previously developed AOW: (a) Cross-section through the rotation axis of the main body of the wheel. (b) Cross-section A-A.

Fig. 3 Motion transmission in differential gear mechanism of AOW: (a) Rotation of input shafts in the same direction. (b) Rotation of input shafts in opposite directions.

Fig. 4 New AOW design with seamless periphery.

Fig. 5 Geometry of barrel-shaped outer roller.

Fig. 6 Maximum available space for outer roller radius: (a) Roller end interference. (b) Roller middle interference.

Fig. 7 Minimum to maximum radius ratio of the outer roller for each number of outer rollers in the AOW. The bold black line indicates the upper limit of the radius ratio. The colored lines show the contour plots of the ratios between the maximum radius of the outer roller and the radius of the main wheel.

Fig. 8 (a) Input angular velocity and (b) acceleration versus rotational angle of the main wheel when the AOW moves diagonally at $v_x = v_y = \sqrt{2}/4$ m/s and $\dot{v}_x = \dot{v}_y = 0$ m/s^2.

Fig. 9 Maximum acceleration of AOW in various different directions when it travels at various speeds in the initial direction. The acceleration indicates the ratio to the value at $v = 0\ \mathrm{m/s}$.

Fig. 10 Omnidirectional movement of the vehicle using the new AOW and a passive omni wheel: (a) Forward translation. (b) Right translation. (c) Right-forward (diagonal) translation. (d) Turning.

Fig. 11 Kinematic model for omnidirectional vehicle with one AOW and one passive omni wheel.

Fig. 12 Singular configuration in the omnidirectional mobile robot, where the center of the AOW is on the wheel plane of the passive omni wheel.

Fig. 13 (a) Developed new AOW. (b) Transmission system inside the AOW.

Fig. 14 Developed two-wheel-drive omnidirectional vehicle with one new AOW and one passive omni wheel

Fig. 15 Control system hardware for developed omnidirectional vehicle

Fig. 16 Mobility testing of developed omnidirectional vehicle: (a) Forward translation. (b) Right translation. (c) Diagonal translation. (d) Turning.

Fig. 17 Measured values of angular velocities ω_1 and ω_2 compared to values

commanded by the AOW controller.

Fig. 18　Variation in the right/left velocity of the vehicle V_X when a 50-ms delay exists between the actual and commanded input angular velocities.

Fig. 19　Measurement results of vertical vibration in vehicle motion: (a) Vibration of the vehicle with the conventional AOW ($f = 6.57$ Hz). (b) Vibration of the vehicle with the new AOW ($f = 1.91$ Hz). The black line indicates Janeway's recommended amplitude limit [25].

Table 1　Number of parts in the conventional and new AOWs

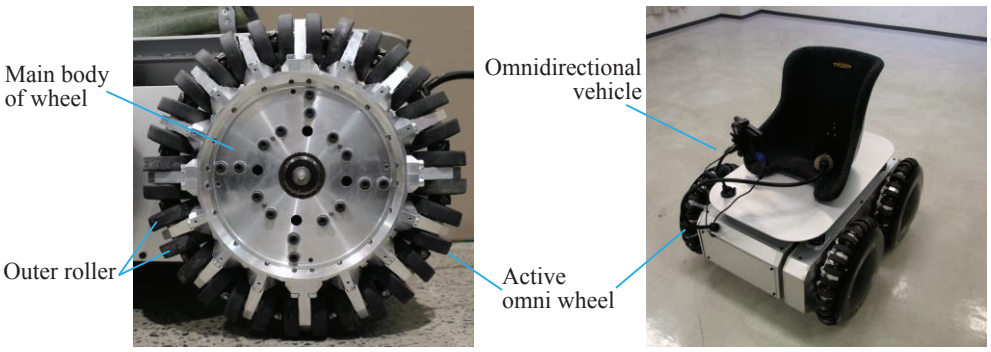

Fig. 1 Active omni wheel and omnidirectional vehicle developed in [23].

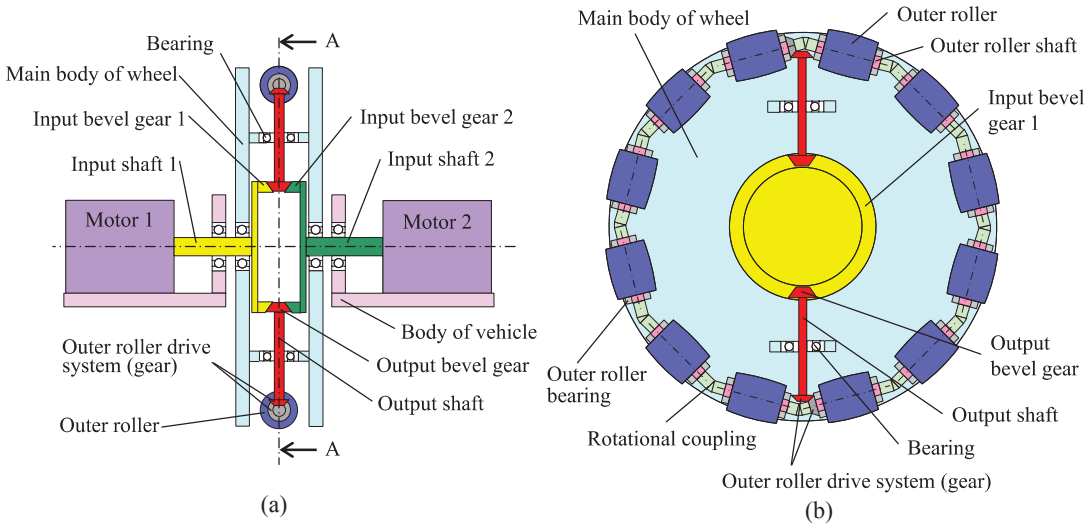

Fig. 2 Structure of previously developed AOW: (a) Cross-section through the rotation axis of the main body of the wheel. (b) Cross-section A-A.

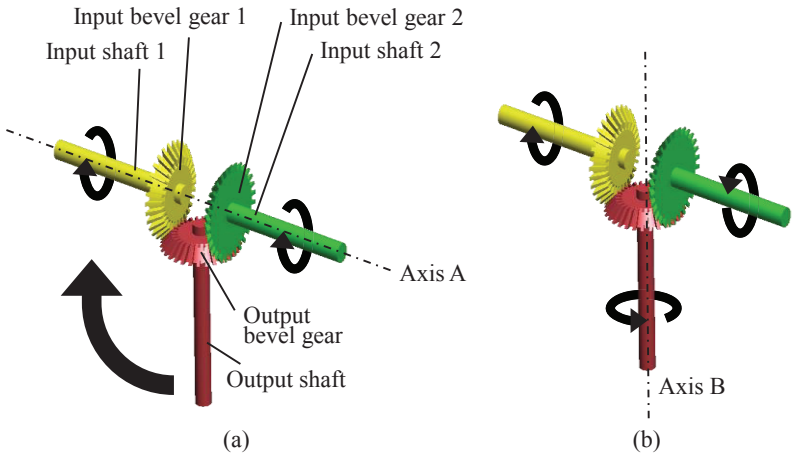

Fig. 3 Motion transmission in differential gear mechanism of AOW: (a) Rotation of input shafts in the same direction. (b) Rotation of input shafts in opposite directions.

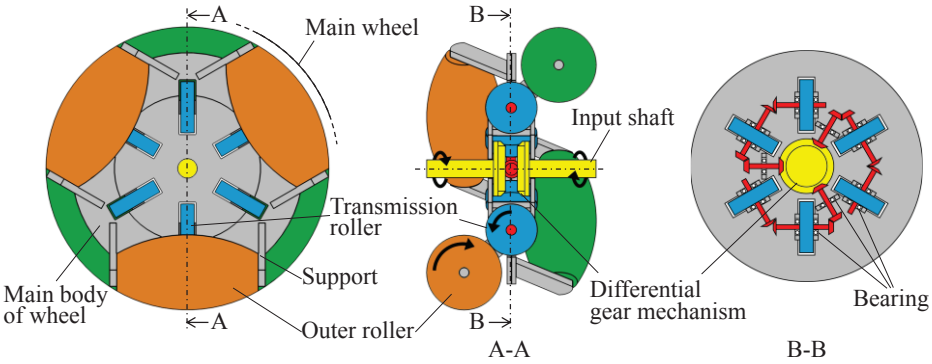

Fig. 4 New AOW design with seamless periphery.

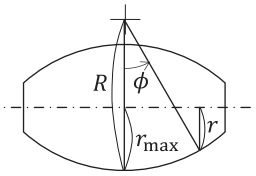

Fig. 5 Geometry of barrel-shaped outer roller.

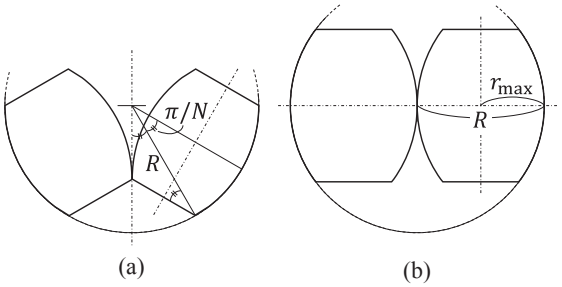

Fig. 6 Maximum available space for outer roller radius: (a) Roller end interference. (b) Roller middle interference.

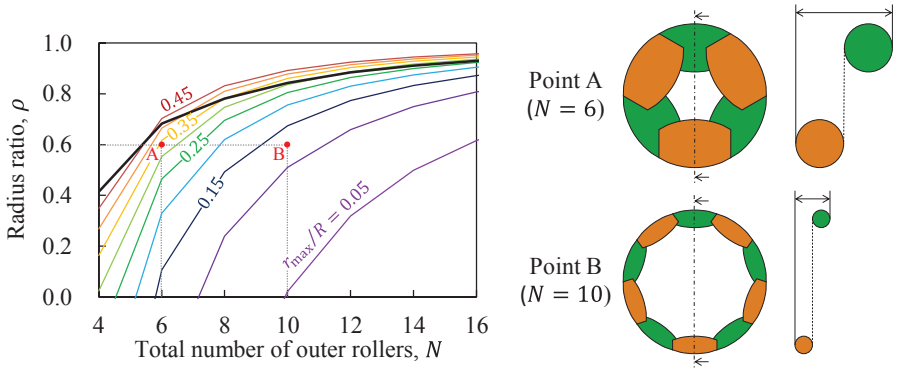

Fig. 7 Minimum to maximum radius ratio of the outer roller for each number of outer rollers in the AOW. The bold black line indicates the upper limit of the radius ratio. The colored lines show the contour plots of the ratios between the maximum radius of the outer roller and the radius of the main wheel.

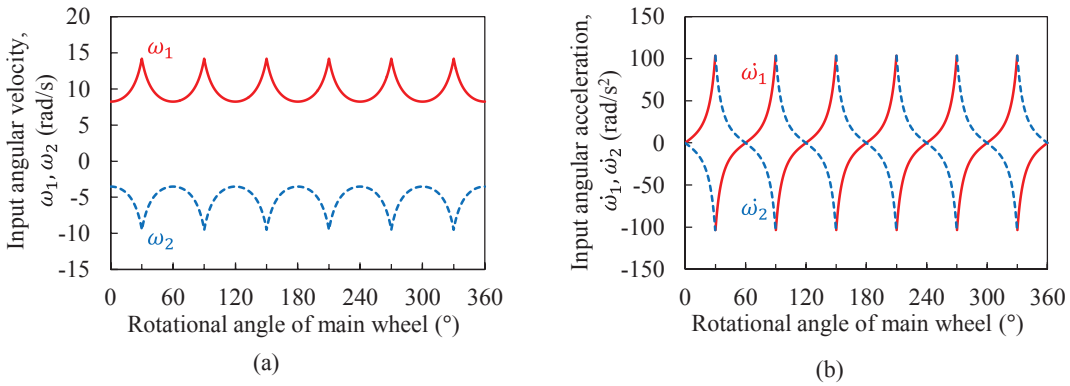

Fig. 8 (a) Input angular velocity and (b) acceleration versus rotational angle of the main wheel when the AOW moves diagonally at $v_x = v_y = \sqrt{2}/4$ m/s and $\dot{v}_x = \dot{v}_y = 0$ m/s².

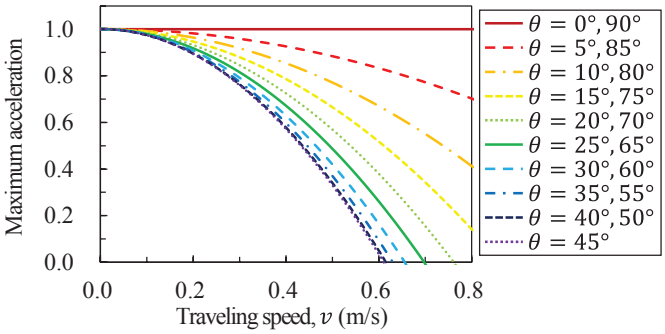

Fig. 9 Maximum acceleration of AOW in various different directions when it travels at various speeds in the initial direction. The acceleration indicates the ratio to the value at $v = 0$ m/s.

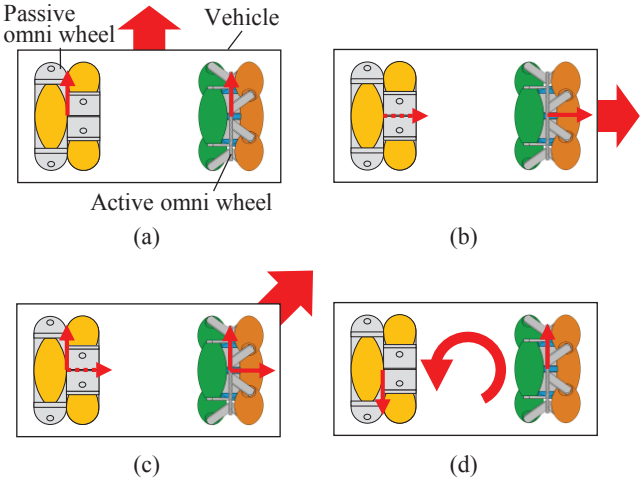

Fig. 10 Omnidirectional movement of the vehicle using the new AOW and a passive omni wheel: (a) Forward translation. (b) Right translation. (c) Right-forward (diagonal) translation. (d) Turning.

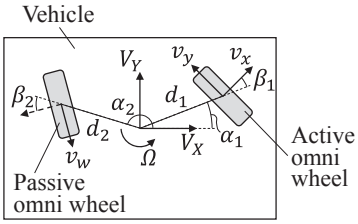

Fig. 11 Kinematic model for omnidirectional vehicle with one AOW and one passive omni wheel.

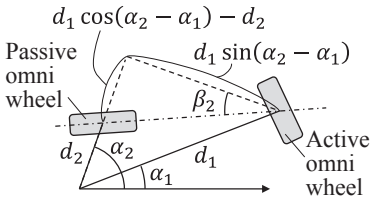

Fig. 12 Singular configuration in the omnidirectional mobile robot, where the center of the AOW is on the wheel plane of the passive omni wheel.

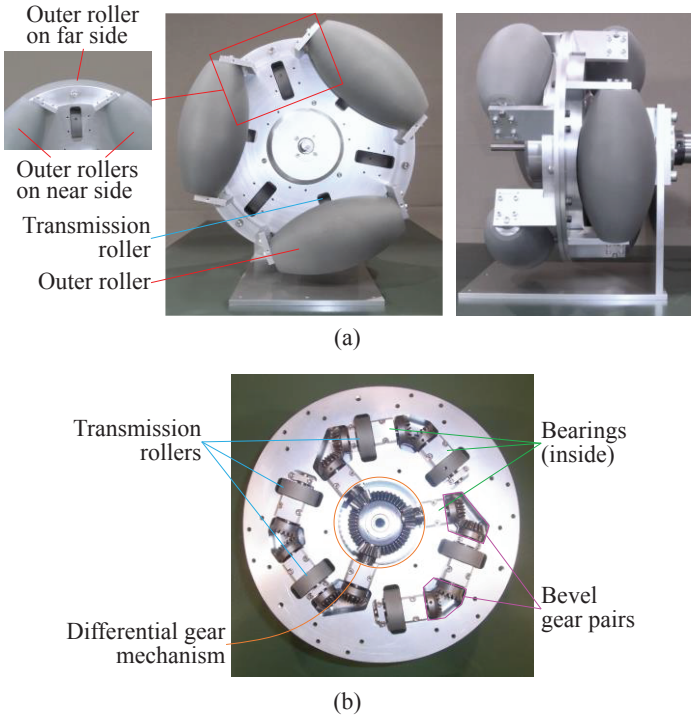

Fig. 13 (a) Developed new AOW. (b) Transmission system inside the AOW.

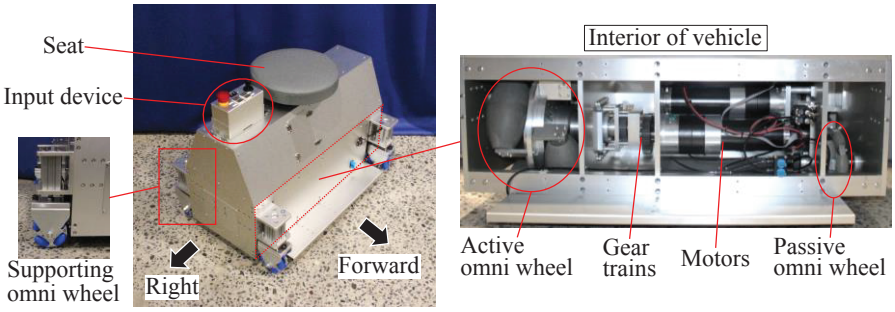

Fig. 14 Developed two-wheel-drive omnidirectional vehicle with one new AOW and one passive omni wheel

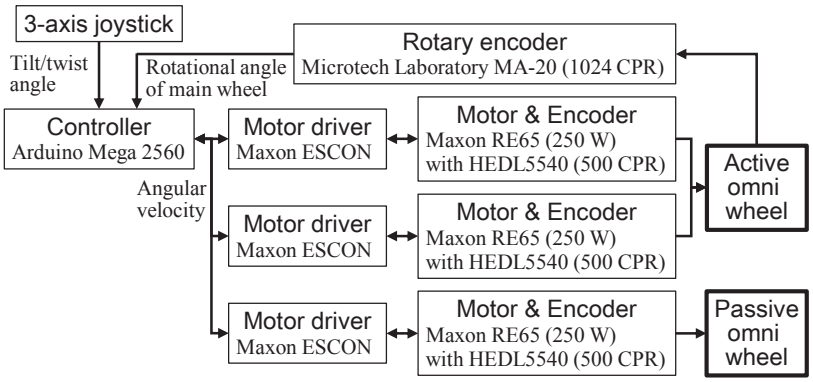

Fig. 15 Control system hardware for developed omnidirectional vehicle

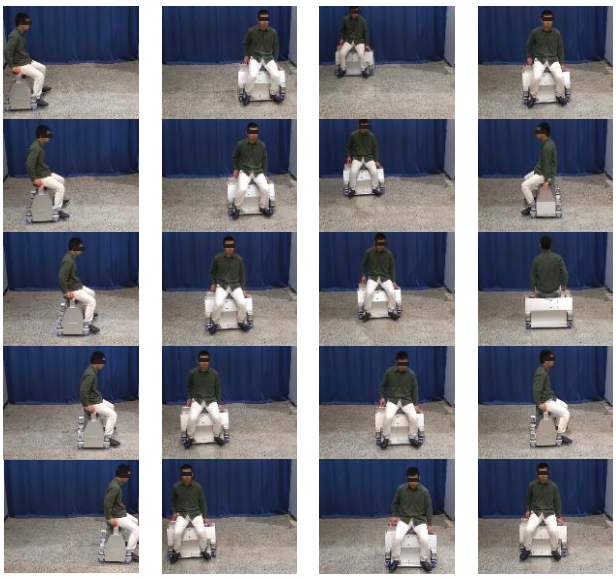

(a) (b) (c) (d)

Fig. 16 Mobility testing of developed omnidirectional vehicle: (a) Forward translation. (b) Right translation. (c) Diagonal translation. (d) Turning.

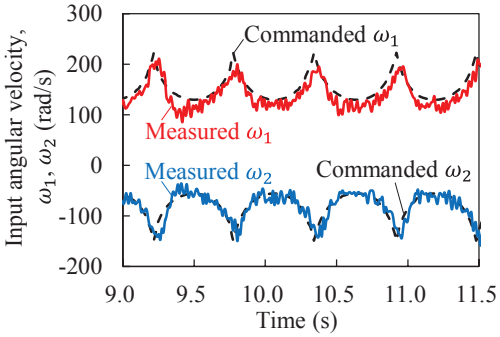

Fig. 17 Measured values of angular velocities ω_1 and ω_2 compared to values commanded by the AOW controller.

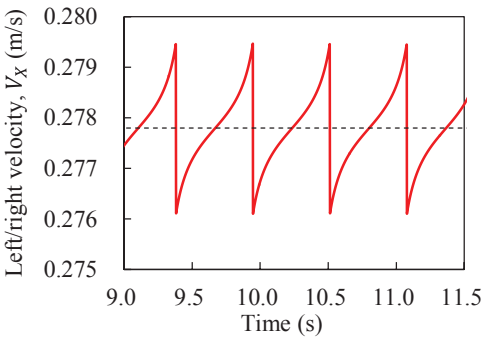

Fig. 18 Variation in the right/left velocity of the vehicle V_X when a 50-ms delay exists between the actual and commanded input angular velocities.

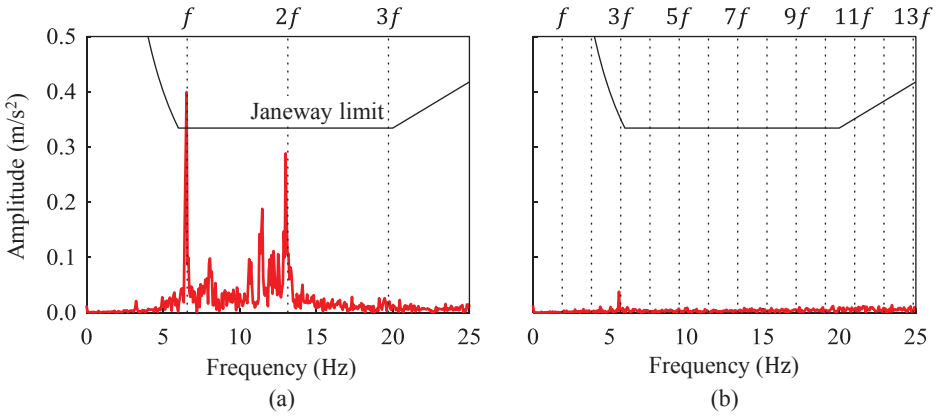

Fig. 19 Measurement results of vertical vibration in vehicle motion: (a) Vibration of the vehicle with the conventional AOW ($f = 6.57$ Hz). (b) Vibration of the vehicle with the new AOW ($f = 1.91$ Hz). The black line indicates Janeway's recommended amplitude limit [25].

Table 1 Number of parts in the conventional and new AOWs

	Conventional AOW	New AOW
Rollers	32	12
Gears	26	17
Couplings	32	0
Shafts	30	17
Outer roller's supports	20	12
Main body	2	2
Total	142	60